Algal Research 100 (2026) 104999

Contents lists available at ScienceDirect

Algal Research

journal homepage: www.elsevier.com/locate/algal

Optimization of the light wavelength composition and illumination intensity profile for the production of the triterpene squalene with engineered *Synechocystis sp.* PCC6803

Leon Poduschnick [a,d], David Mihaescu [a], Andreas Nakielski [b,d], Dennis Dienst [b], Ann-Katrin Beuel [c], Leonie Voß [c], Ilka Maria Axmann [b], Jørgen Barsett Magnus [a,d,*]

[a] Chair of Biochemical Engineering, RWTH Aachen University, Forckenbeckstraß e 51, Aachen, 52074, North Rhine-Westphalia, Germany
[b] Synthetic Microbiology, Biology Department, Heinrich-Heine-Universität Düsseldorf, Universitätsstraß e 1, Düsseldorf, 40225, North Rhine-Westphalia, Germany
[c] Fraunhofer Institute for Molecular Biology and Applied Ecology IME, Forckenbeckstraß e 6, Aachen, 52074, North Rhine-Westphalia, Germany
[d] Bioeconomy Science Center (BioSC), Forschungszentrum Jülich, Jülich, 52425, North Rhine-Westphalia, Germany

ARTICLE INFO

Keywords:
Synechocystis sp. PCC6803
Terpenoids
Squalene
Design of experiments
Illumination
Wavelength composition

ABSTRACT

The spectral composition of the incident light source remains an underutilized asset in the control and optimization of biotechnological production with cyanobacteria. Especially the production of terpenoids, a class of molecules whose metabolic pathways are expected to be considerably affected by the availability and quality of incoming light, could benefit from revised illumination conditions. In this study, we investigated the influence of monochromatic light sources, varying proportions of three different monochromatic light sources, and illumination intensity profiles on growth performance and terpenoid synthesis of a genetically engineered *Synechocystis sp.* PCC6803 squalene producer strain. Biomass and squalene productivity of the strain were increased under broad-spectrum white light illumination compared to monochromatic red and blue light sources of the same intensity. Investigating the impact of different ratios of red, green, and blue LEDs on biomass concentration, we identified an optimal wavelength combination of 60 % red, 0 % green, and 40 % blue light. The squalene concentration was maximized under elevated blue light fractions with a total illumination profile of 44 % red, 0 % green, and 56 % blue light. The supplementation of low-dosage UV-A irradiation increased the cellular carotenoid and squalene load under elevated red light fractions. Hence, with supplemented UV-A irradiation, the optimal wavelength mixture coincided with that for maximized biomass concentration at mixtures of 63 % red, 0 % green, and 37 % blue light. At these conditions, a mean squalene concentration of 48.20 mg L^{-1} (95 % CI [34.80, 61.60] mg L^{-1}) was predicted. Photo-limiting white light illumination intensities increased the cell's squalene load. However, the simultaneous decrease in biomass concentration led to a decrease in total squalene concentrations under lower illumination intensities. These results highlight the potential of adapting the chromatic profile and illumination intensity to boost biotechnological production of terpenoids with cyanobacteria.

1. Introduction

The necessity for illumination is a defining factor for photobioreactor design and process optimization in phototrophic cultivations of cyanobacterial or microalgal strains. Light adds a significant layer of complexity that needs to be controlled and optimized, and is thus often designated as a fourth phase, next to the microorganisms, cultivation medium, and gas bubbles [1,2]. Employing sunlight greatly reduces the associated economic cost compared to artificial lighting, but sacrifices a great deal of possible process control that might be required, especially when producing fine chemicals with these organisms [3]. Primarily, the emission spectrum of the applied light source and the incident illumination intensity affect the photosynthetic efficiency of the cultures and pigment composition of the cells [4,5]. For example, through chromatic acclimation, cyanobacteria regulate the amount and type of the phycobiliproteins that make up the light-harvesting antennas, adapting their structure based on the perceived spectrum of incoming light [6]. In the model organism *Synechocystis sp.* PCC6803 (hereafter *Synechocystis* 6803), the chromatic acclimation is typed as a class I response. This

* Corresponding author at: Chair of Biochemical Engineering, RWTH Aachen University, Forckenbeckstraß e 51, Aachen, 52074, North Rhine-Westphalia, Germany.
E-mail address: jorgen.magnus@avt.rwth-aachen.de (J.B. Magnus).

https://doi.org/10.1016/j.algal.2026.104999
Received 15 June 2026; Received in revised form 8 September 2026; Accepted 7 October 2026
Available online 14 October 2026
2211-9264/© 2026 The Authors. Published by Elsevier B.V. This is an open access article under the CC BY license (http://creativecommons.org/licenses/by/4.0/).
Open access funding enabled and organized by Projekt DEAL.

class is characterized by the redistribution of light energy between photosystems under green and red light by adjusting the amount of rod-shaped versus hemidiscoidal phycobilisomes that primarily attach to either photosystem I or II via specific linker proteins [7–9]. Contrary to other chromatic acclimation types, the production of major phycobiliproteins in these strains remains constant under varying ambient lighting conditions [5]. In addition to changes to the light-harvesting apparatus, some substrains of the *Synechocystis* 6803 wildtype can adjust to different light conditions by means of phototaxis [10–12]. Generally, for cultivations of *Synechocystis sp.*, red light is beneficial for growth, while the organisms show decreased growth rates under blue light. The decrease in growth rate under blue wavelengths is primarily caused by an excitation imbalance between photosystems I and II, and the absence of phycocyanin absorbance at these wavelengths [12–15]. In conjunction with the quality of the applied light, the quantity plays a crucial role as well [16]. While optimal incident illumination intensities are specified to be in the range of 10 $\mu mol_{Photons}\ m^{-2}\ s^{-1}$ to 250 $\mu mol_{Photons}\ m^{-2}\ s^{-1}$ for most cultivation strategies of cyanobacteria, the actual optimal illumination intensity is highly dependent on the geometry of the applied photobioreactor. The cell-specific illumination intensity further changes during the cultivation due to differences in the spatial position of the cell inside the bioreactor and changes to light attenuation based on the cyanobacterial extinction coefficient and culture density [17–19]. In an ideal set-up, the illumination intensity would be maintained near the photosaturation point to maximize both productivity and photosynthetic yield [20].

Concurrently with adapting their photosynthetic apparatus in response to varying light conditions, certain light regimes can alter carbon partitioning in cyanobacteria and microalgae, favoring some metabolic routes over others. The effects are, however, strongly dependent on the considered microorganism and lighting conditions. For example, it has been found that red light enhances growth, while blue light stimulates oil formation in the green algae *Chlorella vulgaris* [20]. Contrarily, lipid accumulation in the cyanobacterium *Cyanobium sp.* is reported to increase with red or green light supplementation and decrease under UV or blue light [21]. Irradiation with red light also enhances the lipid content in *Nannochloropsis gaditana* compared with blue light [2]. The same applies to the lipid and carbohydrate content in *Microcystis aeruginosa* [22]. Production of carotenoids, a group of pigments with antioxidative properties, is upregulated in *Haematococcus pluvialis* by blue and UV light irradiance [23]. As a major stressor for phototrophic cells, generally inducing the formation of reactive oxygen species, UV radiation also enhances carotenoid accumulation in the cyanobacterium *Leptolyngbya* cf. *fragilis* [24,25]. Additionally, carotenoid accumulation in *Synechocystis salina* and *Synechocystis* 6803 is primarily increased by high intensities of white light and not individual light colors [26–28], although some authors report an increase in carotenoid content during red light irradiance for *Synechocystis* 6803 [13]. Collectively, these studies indicate great potential for process optimization concerning the intensity and quality of artificial lighting in microalgal and cyanobacterial cultivations for biotechnological production.

Photoautotrophic organisms are particularly interesting hosts for synthesizing terpenoids. This large class of molecules includes, among others, the phytol tail of the cyanobacterial pigment chlorophyll *a* and carotenoids. Their diversity and usual structural complexity entail a broad range of potential applications in chemical and pharmaceutical industries [29–31]. One interesting target terpenoid is the triterpene squalene that has use cases in the pharmaceutical industry as a vaccine adjuvant, as well as in cosmetic and nutritional industries as a skin protectant and antioxidant [32]. Usually, chemical synthesis of terpenoids is difficult and costly, which makes natural producers like plants or potentially cyanobacteria interesting sources despite typically low product yields [33,34]. For squalene specifically, most of the global demand is still sourced from shark-liver oil, setting an additional precedent for biotechnological production due to environmental and ethical concerns [32,35]. This sustainability challenge led to metabolic engineering efforts for squalene production in different cyanobacterial strains like *Synechococcus elongatus* [36,37] and *Synechocystis* 6803 [35,38]. In cyanobacteria, terpenoids are synthesized via the methyl-erythritol-phosphate (MEP) pathway, the regulation of which is expected to be tightly coupled to photosynthetic activity [30,33,39]. The presumption that light-dependent activity of the MEP pathway can be exploited to elevate productivity has recently been substantiated by a study showing increased production of the terpene precursor isoprene with engineered *Synechocystis* 6803 under illumination with violet light [40].

The wavelength-dependence of strain productivity has only recently gained attention. Furthermore, those studies focus on the effect of monochromatic light on cyanobacterial growth and production of chemicals, while the effects of combining wavelengths from distant spectral regions have not been systematically investigated. In this study, we explore the influence of different mixtures of red, blue, and green light on biomass and squalene production by an engineered *Synechocystis* 6803 strain using statistically planned experiments. Furthermore, we assess the impact of low-dosage UV-A supplementation on pigmentation and squalene production. Lastly, we test the impact of different maximum incident illumination intensities on photo-limited and photo-saturated growth in induced and uninduced producers. These results will lay the groundwork for optimizing and controlling the process of producing squalene with cyanobacteria.

2. Material and methods

2.1. Microbial strain and cryo preservation

We utilized a *Synechocystis* strain engineered for enhanced squalene production. This strain was developed from the previously published *Synechocystis Δshc* NS2::P_{rha} *sqs* strain [35], which overexpresses the native squalene synthase (*sqs*, gene locus *sll0513*) gene under the control of the L-rhamnose-inducible promoter P_{rha}.

For effective rhamnose-mediated induction of P_{rha}, the *rhaS* gene, encoding the RhaS activator protein, was ectopically expressed from the RSF1010-based, self-replicative plasmid pSNDY under the control of the constitutive synthetic promoter P_{J23119}.

To further boost squalene biosynthesis, three native MEP (methylerythritol phosphate) pathway genes, encoding 1-deoxy-D-xylulose-5-phosphate synthase (*Dxs*, gene locus *sll1945*), IPP/DMAPP isomerase (*Idi*, gene locus *sll1556*) and 2-C-methyl-D-erythritol-2,4-cyclodiphosphate reductase (*IspG*, gene locus *slr2136*), were arranged as a tricistronic operon on the pSNDY-*rhaS* plasmid. Operon expression was also driven by the P_{rha} promoter. These additional overexpression targets have previously been shown to increase isoprene or terpenoid production in *Synechocystis* 6803 [41,42]. For further details on the expression constructs, see supplementary material, Figure S1. Additionally, a detailed summary of all used genetic modules is given in the supplementary material, Table S1.

The strain was preserved in cryo cultures as 1 mL aliquots at −80 °C. Cryo cultures were prepared by centrifuging freshly grown preculture at 14 000 RPM for 10 min. The resulting cell pellet was resuspended in cultivation medium with 8 % DMSO in water to an optical density at 750 nm of 5.

2.2. Growth medium

The growth medium for high cell-density cultivation of cyanobacteria was adapted from [43]. We omitted $CuSO_4$ from the medium and $CoCl_2$ was exchanged for $Co(NO_3)_2$ in the trace element solution at the same molar concentration. Additionally, TES-KOH buffer was added to a final concentration of 50 mM at a pH of 8. Overall, the initial medium was comprised of 50 mM $NaNO_3$, 50 mM TES buffer,

4 mM K_2HPO_4, 2.5 mM $KHCO_3$, 2 mM $MgSO_4$, 50 µM $CaCl_2$, 150 µM Na_2–EDTA, 150 µM $FeCl_3$, with additional trace elements consisting of 25 µM $B(OH)_3$, 20 µM $MnCl_2$, 2 µM $ZnSO_4$, 3 µM Na_2MoO_4, and 60 nM $Co(NO_3)_2$. Every component except for $FeCl_3$, which was stored in solution together with Na_2–EDTA, and the trace element mix was stored in a separate concentrated stock solution. Stock solutions were either sterilized by filtration over a membrane with a pore size of 0.2 µm or by autoclaving at 121 °C for 20 min. The Fe-EDTA solution, $KHCO_3$ solution, and the trace element mix were stored at 4 °C while the remaining solutions were stored at room temperature. Prior to each experiment, the cultivation medium was prepared from the individual stock solutions and sterilized de-ionized water.

In main cultures, L-rhamnose was added to a final concentration of 5 mM to induce product synthesis. Moreover, in every cultivation, the antibiotics chloramphenicol and nourseothricin were added as selection agents to a final concentration of 10 µg mL^{-1} and 25 µg mL^{-1}, respectively.

2.3. Cultivation conditions

Main cultures were grown either in shake flasks to study the light-color effects or in microtiter plates to assess the influence of incident white-light intensity. Precultures were inoculated from cryo stocks and grown in the same system under the same culture conditions as the respective main culture. However, all precultures were maintained under white light illumination.

Cultivation at shake flask scale was carried out in 100 mL Erlenmeyer flasks filled with 15 mL of growth medium and inoculated to an initial optical density at 750 nm of 0.1. To ensure stable cultivation conditions, an incubation hood was used and set to a controlled temperature of 30 °C. The light was provided by an LEDitSHAKE module [44,45] in the form of blue (451 nm, Oslon SSL 120 Deep Blue, OSRAM, Germany), red (660 nm, Oslon SSL 120 Hyper Red, OSRAM, Germany), green (528 nm, Oslon SSL 80 Green, OSRAM, Germany), white (Square 120 CRI90+ 5700 K, OSRAM, Germany), and UV-A LEDs (365 nm, SSC VIOSYS UV CUN66A1B, Republic of Korea), either individually or in combination. In all cases, the total incident illumination intensity was maintained at 30 µmol$_{Photons}$ m^{-2} s^{-1} or 40 µmol$_{Photons}$ m^{-2} s^{-1}. In the LEDitSHAKE module, external light was blocked by black plastic sheaths around each shake flask. The flasks were shaken at 150 RPM and a shaking diameter of 50 mm. The cultures were individually gassed with 1.5 % CO_2 and 98.5 % synthetic air. The system allowed the cultivation of up to 8 flasks in parallel.

Cultivations in microtiter plate scale were conducted with a micro respiratory activity monitoring system (µRAMOS) combined with a custom-made LED module [46,47]. We used black polypropylene 48-deep-well microtiter plates with a transparent polystyrene bottom (M2P-MTP-R48-B, Beckmann Coulter, USA) for each cultivation. All 48 positions of the microtiter plates were fitted with a white light LED whose intensity could be controlled individually. We used a culture volume of 1 mL per well and inoculated the growth medium to an optical density at 750 nm of 0.1 at the start of each experiment. The system was placed inside a temperature-controlled incubation hood set to 30 °C. The microtiter plate was shaken at 700 RPM at a shaking diameter of 3 mm. Cultures were actively gassed with 5 % CO_2 and 95 % synthetic air by the µRAMOS system.

2.4. Biomass determination

The optical density was measured at 750 nm using a spectrophotometer (20 Genesys, Thermo Scientific, USA). Measurements were zeroed against a 0.9 % (w/v) NaCl solution. Individual samples were diluted with the same solution to fall within the previously determined linear range of the measuring device of 0.1 to 0.3.

The cell-dry weight was determined from 1 mL-samples of culture broth. The samples were centrifuged at 14 000 RPM for 10 min. Cell pellets were separated from the supernatant and dried in pre-weighed reaction tubes at 80 °C for 24 h. After acclimatization to room temperature in a desiccator for 1 h, the mass of the cell pellet was measured on an analytical balance and corrected by subtracting the empty tube mass.

2.5. Quantification of pigments

To determine the concentrations of chlorophyll *a* and carotenoids, a defined aliquot of the culture broth was centrifuged at 14 000 RPM for 5 min. After discarding the supernatant, cell pellets were solubilized in 1 mL of methanol that was cooled to 4 °C. Samples were incubated for 30 min at 4 °C and 100 RPM in a ThermoMixer C (Eppendorf, Germany). The sample was centrifuged again at 14 000 RPM for 5 min. From 100 µL of supernatant, the absorbance at 470 nm, 665 nm, and 720 nm was quantified in a plate reader (Synergy 4, BioTek, USA). Samples were zeroed against methanol and diluted with methanol if the absorbance would have otherwise exceeded 0.2. Additionally, one sample was measured in a spectrophotometer (20 Genesys, Thermo Scientific, USA) to correct measurements for the difference in optical path length between the spectrophotometer and the plate reader. The concentrations of chlorophyll *a* and carotenoids were then calculated with the following formulas based on the corrected absorption for an optical path length of 1 cm [48,49]:

$$\text{Chl } a = 12.9447 \cdot \left(A_{665\,nm} - A_{720\,nm}\right) \quad \left[\text{mg L}^{-1}\right] \tag{1}$$

$$\text{Carotenoids} = \frac{1000 \cdot \left(A_{470\,nm} - A_{720\,nm}\right) - 2.86 \cdot \text{Chl } a\,\left[\text{mg L}^{-1}\right]}{221} \quad \left[\text{mg L}^{-1}\right] \tag{2}$$

2.6. Quantification of squalene

Squalene was extracted from a cell pellet that was separated from a defined aliquot of culture broth via centrifugation at 14 000 RPM for 5 min. The cell pellet was incubated for 10 min at 50 °C with 500 µL of acetone that contained an internal standard for quantification. The internal standard was composed of 25 µM beta-sitosterol for gas chromatography coupled mass spectrometry (GC-MS) and 500 mg L^{-1} octadecyl benzene for high-performance liquid chromatography (HPLC) measurements. After the incubation period, 500 µL of 1 M NaCl solution were added, and the sample was vigorously mixed at 2000 RPM for 1 min. Next, 500 µL of n-hexane was added, and the mixture was shaken again at 2000 RPM for 1 min. The aqueous and organic phases were separated via centrifugation at 14 000 RPM for 5 min. The squalene concentration was quantified either directly from the n-hexane overlay via GC-MS, or n-hexane was exchanged for acetonitrile/tetrahydrofuran (9:1, v/v) for measurement with HPLC. To calibrate the HPLC or GC-MS measurement, five defined concentrations of squalene in n-hexane (10 mg L^{-1} to 500 mg L^{-1} for HPLC and 5 mg L^{-1} to 200 mg L^{-1} for GC-MS) were subjected to the same respective extraction protocol as described earlier for the samples. This was done to account for the phase partition coefficients as well as potential evaporative and oxidative loss of squalene during the procedure. Both calibration curves had an R^2 of 0.99. The applied method of squalene quantification is indicated in each figure and table caption.

For the GC-MS measurement, 1 µL of sample was injected in splitless mode onto a GC column (19092S-433UI, 30 m × 250 µm × 0.25 µm, Agilent Technologies, USA). The temperature of the column oven was initially set to 70 °C and then increased at a rate of 42 °C min^{-1} to 280 °C. Afterwards, the temperature was further increased at a rate of 4 °C min^{-1} to 320 °C. The endpoint temperature was held for 4 min at the end of the program. Helium was employed as the mobile phase at a constant flow rate of 0.8 mL min^{-1}. The concentration of analytes was assessed via a mass spectrometer (Agilent 5977 MSD, Agilent

Technologies, USA). Electron impact ionization was used at 70 eV and a source temperature of 230 °C.

For HPLC analysis, the n-hexane was evaporated over approximately 24 h under a fume hood at room temperature. Afterwards, the residue was redissolved in 200 µL acetonitrile/tetrahydrofuran (9:1, v/v) by vortexing. The HPLC method was adapted from [50] with minor changes. Briefly, 1 µL of sample was injected onto an HPLC column (Nucleodur 100-5 C18 ec, 5 µm, 250 mm × 4.6 mm, Macherey-Nagel, Germany) and analytes were separated at 35 °C with a constant flow rate of 0.8 mL min^{-1} of a mobile phase consisting of acetonitrile/tetrahydrofuran (8:2, v/v). Additionally, a precolumn (SecurityGuard C18, 4 mm × 3.0 mm ID, Phenomenex, USA) was employed in the method. Analytes were detected and quantified with a photodiode array detector (SPD-20 A, Shimadzu, Japan) at 220 nm.

2.7. Design of experiments

Designed experiments were planned and analyzed with JMP Student 18 (JMP Statistical Discovery LLC, USA). We conducted two different-designed experiments for this study. The experimental design for the investigation of the effect of different wavelength compositions of the applied light consisted of three blocks with eight experimental runs each. The runs were distributed based on the D-optimality criterion [51] with two center points being forced in. We included the ratio of the intensity between a red (660 nm), blue (451 nm), and green (528 nm) LED as a mixture variable in the design. We allowed all possible combinations, for which the illumination intensities of the photosynthetically-active radiation summed up to 40 $\mu mol_{Photons}\ m^{-2}\ s^{-1}$ in total. Additionally, UV-A light supplementation (365 nm) at an intensity of 1 $\mu mol_{Photons}\ m^{-2}\ s^{-1}$ was included as a categorical process variable, meaning it could only be either active or inactive during cultivation. To account for possible batch-to-batch variations, the experimental block was included as a random variable as well. We used Eq. (3) as the model to generate the experimental plan with the "custom design" platform of JMP. Here, a standard Scheffé cubic model [52] was crossed with the process variable of UV light in the linear terms. This type of model is generally referred to as a Kowalski-Cornell-Vining (KCV) model and marks a compromise between a fully crossed and fully additive model that combines mixture and process variables [53]. In Eq. (3), α denotes the parameter set for the Scheffé cubic model, δ the parameter set for the asymmetric blending terms, and γ the set of parameters for the crossed linear terms. The variable sets for the mixture and process variables are defined as z and x, respectively.

$$y(x,z) = \sum_{k=1}^{3} \alpha_k \cdot z_k + \sum_{k<l}^{2} \sum_{k}^{3} \alpha_{kl} \cdot z_k z_l + \sum_{k<l}^{2} \sum_{l}^{3} \delta_{kl} \cdot z_k z_l \left(z_k - z_l\right) + \alpha_{\mathrm{Red,Blue,Green}} \cdot z_{\mathrm{Red}} z_{\mathrm{Blue}} z_{\mathrm{Green}} + \sum_{k=1}^{3} \gamma_{k,\mathrm{UV}} \cdot z_k x_{\mathrm{UV}} \quad (3)$$

While the experimental plan was initially designed based on the function that is depicted in Eq. (3), we also tested whether a reduced KCV model based on a Scheffé quadratic model [52] could adequately describe our observations without compromising model accuracy for every tested response (comparable or better adjusted R^2). This was done to not overfit the observed data. All R^2 values reported in the text refer to the unadjusted values. The adjusted values R^2_{adj} are given in the supplementary material, Table S3-S12. The reduced KCV model is given in Eq. (4).

$$y(x,z) = \sum_{k=1}^{3} \alpha_k \cdot z_k + \sum_{k<l}^{2} \sum_{k}^{3} \alpha_{kl} \cdot z_k z_l + \sum_{k=1}^{3} \gamma_{k,\mathrm{UV}} \cdot z_k x_{\mathrm{UV}} \quad (4)$$

Because the random block effect was retained for all models, the final KCV models were fit with restricted maximum likelihood (REML) estimation. We performed a Wald test with the unbounded variance component estimates of the random block effect and residual to assess whether block-to-block variation was significant for every model.

The second designed experiment included the slope of the intensity increase and the endpoint incident illumination intensity of a white LED as continuous process variables. Also, the status of induction of product synthesis was included as a categorical process variable with two levels (induced, not induced). The considered model is depicted in Eq. (5). Based on this model, 48 runs were distributed based on the I-optimality criterion by the optimization algorithm of JMP [51]. Here, the response models were fit using ordinary least squares regression. We included all linear and quadratic terms except for the pure quadratic term of the categorical variable of the induction status. In Eq. (5), the parameter set is defined as β, while the variable set is termed as x.

$$y(x) = \beta_0 + \sum_{i=1}^{3} \beta_i \cdot x_i + \sum_{i<j}^{2} \sum_{j}^{3} \beta_{ij} \cdot x_i x_j + \sum_{i=1}^{2} \beta_{ii} \cdot x_i^2 \quad (5)$$

Optical density (OD_{750}), squalene concentration (mg L^{-1}), squalene load, chlorophyll *a* load, and carotenoid load (all mg L^{-1} OD_{750}^{-1}) were investigated as responses y for all experiments.

3. Results and discussion

3.1. Effect of white light compared to monochromatic red and blue light on growth and squalene synthesis

Although monochromatic light affects cyanobacterial physiology and productivity, the impact of mixtures of monochromatic light ratios on growth and product synthesis remains unexplored. To address this, we compared the volumetric productivities of engineered *Synechocystis* cultures under conventional white light illumination versus monochromatic red and blue light. This approach benchmarks wavelength-specific effects against standard broad-spectrum light conditions. The engineered *Synechocystis* 6803 was cultured in Erlenmeyer flasks within an LEDitSHAKE module [44,45]. At each flask position, six LEDs provided independent control of the illumination intensity and emission spectrum. The flasks were individually illuminated by white, red (660 nm), or blue (451 nm) light at an intensity of 30 $\mu mol_{Photons}\ m^{-2}\ s^{-1}$. The oxygen evolution and carbon dioxide consumption of each culture were monitored with a RAMOS device [54]. We assumed photosaturation in regions where the oxygen production rate stayed constant for the rest of the experiment (Figure S2). During the photosaturated regime, each condition was sampled at three different sampling time points. Fig. 1 shows the respective biomass and squalene production rates fitted from this data set. Additionally, the biomass-specific (OD_{750}) squalene concentration (squalene load) was calculated from the quotient of the volumetric biomass and squalene productivities.

Biomass productivity was highest under illumination with white light, while blue light irradiation showed the lowest biomass productivity at 0.67 ± 0.10 $OD_{750}\ d^{-1}$. Biomass productivity under red light was slightly lower than under white light, at a productivity of 1.15 ± 0.14 $OD_{750}\ d^{-1}$ compared to 1.61 ± 0.02 $OD_{750}\ d^{-1}$, respectively. It is well-established in literature that red light illumination can be more efficiently utilized for growth by *Synechocystis* 6803 than blue light [13,55,56]. This effect is associated with a lack of absorption of phycobilisomes at blue wavelengths, which causes an excitation imbalance between photosystems I and II [15]. Comparisons between biomass productivities under broad spectrum and narrow-wavelength irradiation are not readily available for *Synechocystis* 6803, though Bland et al. (2016) [56] report slightly higher maximum growth rates under allophycocyanin (660 nm) or phycocyanin (620 nm) targeting light than under white light. Singh et al. (2009) [55] observed near-identical growth between *Synechocystis* 6803 grown under red and white light. Models have recently been developed to describe how light source

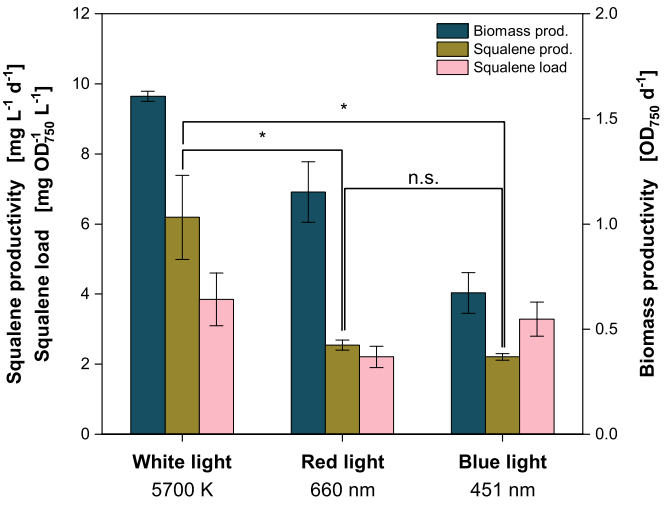

Fig. 1. Comparison between biomass and squalene productivity during light-saturated cultivation with different narrow-wavelength LEDs. Cultures were illuminated with 30 $\mu mol_{Photons}\ m^{-2}\ s^{-1}$ of white, red (660 nm), or blue (451 nm) light. For each condition, three different time points during the light-saturated regime were sampled as biological duplicates. These samples were used for linear regression with OriginPro. Error bars show the standard error of the respective parameter in the linear regression analysis. We tested for significant differences between the data sets by pairwise comparison, including the light color as a variable for the regression analysis. Significant effects (ANOVA, * $p < 0.05$) of the light color on the regression line slope are highlighted in the plot. The squalene concentration was determined by the GC-MS method described in Section 2.6.

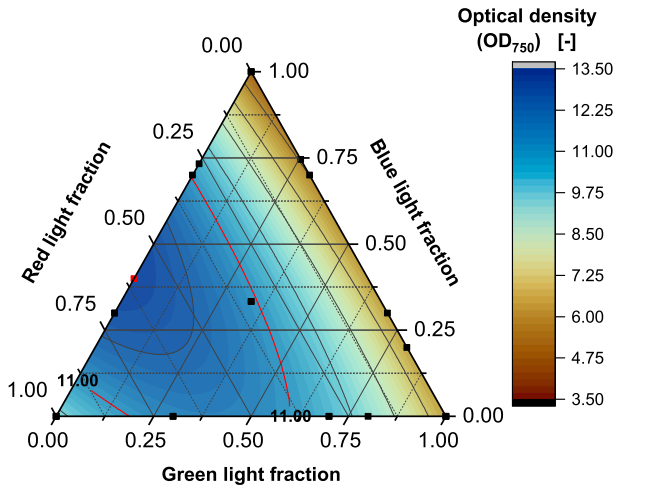

Fig. 2. Contour plots of model predictions for the endpoint optical density of cultivations with different wavelength compositions. In total, the photosynthetically active illumination intensity sums up to 40 $\mu mol_{Photons}\ m^{-2}\ s^{-1}$ for all conditions. A varying amount of red (660 nm), blue (451 nm), or green (528 nm) light was provided to the culture. The model was fit based on Eq. (4) with parameters $\gamma_{k,UV}$ set to 0. A summary of the model parameters is given in the supplementary material, Table S3. The studentized residuals are plotted in the supplementary material, Figure S6A. Overall, 23 data points were used that were randomly distributed into 3 separate experimental blocks. Settings of the performed experiments are indicated by black squares in the plot. The predicted optimum is highlighted by a red square.

emission spectra affect the photosynthetic apparatus of *Synechocystis sp.* PCC6803 [57]. However, the study provides a comparison between simulated responses to different broad-spectrum light sources, but no comparison between irradiation with monochromatic and broad-spectrum light. Generally, the optimal illumination profile is highly strain-specific and is even expected to differ significantly between substrains [12]. Thus, it is expected that a genetically engineered strain will behave differently from the wildtype, especially when synthesizing products that are highly associated with pigment synthesis, like terpenoids [31,33].

Interestingly, while biomass productivity was much higher under red light than under blue light, the squalene productivity was nearly identical under both tested conditions. Accordingly, the squalene load is higher under blue light ($3.29 \pm 0.49\ mg\ OD_{750}^{-1}\ L^{-1}$) than under red light ($2.21 \pm 0.30\ mg\ OD_{750}^{-1}\ L^{-1}$). On the other hand, volumetric squalene productivity was significantly higher at $6.19 \pm 1.20\ mg\ L^{-1}\ d^{-1}$ under illumination with white light compared to both blue and red light. This effect appears to be caused by white light integrating both the elevated biomass productivity observed under red light and the higher cellular squalene load under blue light. However, as white light entails a continuous wavelength spectrum, the effect of other light colors, for example, green light, cannot be excluded based on these results.

3.2. Optimization of the wavelength composition of the light source for squalene production and growth

To investigate the effect of varying proportions of monochromatic light at a constant total illumination intensity on growth and product synthesis, we performed a series of designed experiments in shake flasks. Since near-UV radiation was shown to increase isoprene production in *Synechocystis* 6803 and low UV radiation is associated with the upregulation of other terpenoids like photo-protective carotenoids in cyanobacteria [58,59], we further investigated the effect of illuminating cultures with additional UV-A light (365 nm, 1 $\mu mol_{Photons}\ m^{-2}\ s^{-1}$) on culture performance. In total, 24 cultivations were conducted and randomly distributed into three separate experimental blocks, with each cultivation lasting for approximately 7 d. We excluded some suspected outliers from the fit of the primary models presented in this chapter. The full data set with highlighted excluded points is given in the supplementary material, Table S2. Additionally, Table S7 compares regression statistics for the models fitting the full and reduced data sets for each examined response. The contour plots for the model predictions of the response models utilizing the full data set are given in the supplementary material, Figures S3-S5, to enable a comparison of how the exclusion of the suspected outliers changes the model predictions.

Fig. 2 shows the contour plot for the predicted endpoint optical density for different combinations of red, blue, and green monochromatic light sources. Since the supplementation of UV-A light had no significant effect in the original full model (Eq. (3)), the factor was excluded in favor of a reduced model for this response. The reduced model had an R^2 of 0.92 and exhibited an overall significant fit at a p-value of < 0.0001. The R^2 gives a measure of how much of the observed variance can be attributed to the model compared to random error. A value closer to zero suggests that the model is marginally better at predicting the response than the observed response mean, while a value of 1 implies that the proposed model can perfectly describe the observed data. The p-value gives the significance for a hypothesis test that all parameters of the model, except the intercept, are zero ($y(x) = \beta_0$). The model predicts an optimal setting of approximately 60 % red, 0 % green, and 40 % blue light illumination, which is expected to result in a mean optical density of 12.84 with a 95 % confidence interval (CI) of [11.49, 14.19]. However, there is a large region where the endpoint optical density is expected to reach mean values of at least 11, which is highlighted in the plot. The rate of change concerning the endpoint optical density for any light color inside this region is lower than outside of it, suggesting minimal expected difference in endpoint optical density for factor combinations encompassed by it. The position of this region emphasizes the importance of red light to reach high

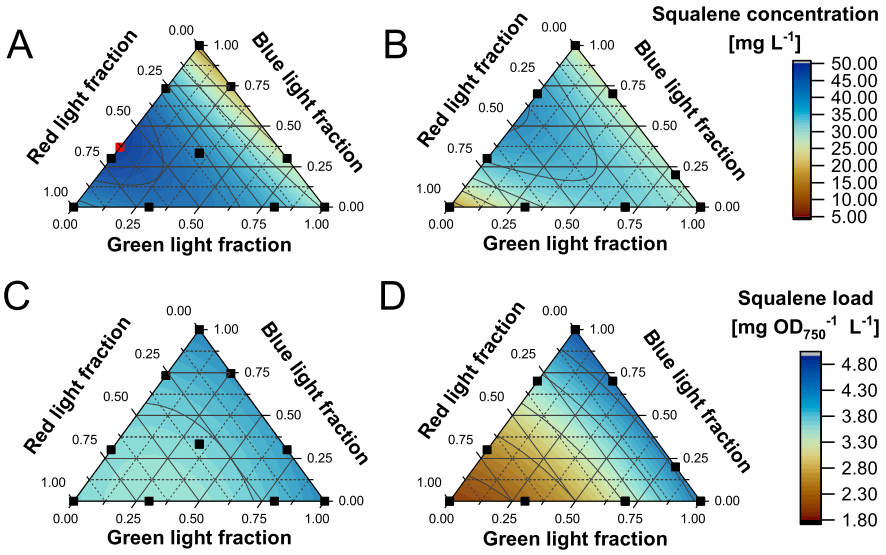

Fig. 3. Contour plots of model predictions for the endpoint squalene concentration (A and B) and squalene load (C and D) of cultivations with different wavelength compositions. In total, the photosynthetically active illumination intensity sums up to 40 $\mu mol_{Photons}\ m^{-2}\ s^{-1}$ for all conditions. A and C: UV-A light (365 nm) was supplied to the culture at an illumination intensity of 1 $\mu mol_{Photons}\ m^{-2}\ s^{-1}$; B and D: No UV-A light supplementation. A varying amount of red (660 nm), blue (451 nm), or green (528 nm) light was provided to the culture. The squalene concentration was determined via the GC-MS method described in Section 2.6. The model was fit based on Eq. (4). Summaries of the model parameters are given in the supplementary material, Table S4 and S5. The studentized residuals are plotted in the supplementary material, Figure S6B and C. Overall, 22 data points were used that were randomly distributed into 3 separate experimental blocks. Settings of the performed experiments are indicated by black squares in the plot. The predicted maximum squalene concentration is highlighted by a red square.

endpoint optical densities, as no factor combination with less than approximately 30 % red light falls into this region. It, however, also confirms the results presented in Fig. 1 as the predicted endpoint optical density decreases again for red light fractions that exceed 60 % of the total incident illumination, thereby solidifying that monochromatic red light yields worse growth performance compared to mixtures of red and blue or red, green, and blue light. This effect could be caused by a comparatively high sensitivity of the genetically engineered strain to elevated illumination intensities of red light, since *Synechocystis* 6803 has been shown to be more sensitive to monochromatic light compared to broad-spectrum illumination in the past [56], and preceding squalene producers were found to be more prone to photo-inhibition in general [35]. However, the rather low total illumination intensity of 40 $\mu mol_{Photons}\ m^{-2}\ s^{-1}$ that was imposed by the cultivation set-up suggests a beneficial effect of blue or green photons as opposed to an adverse effect of elevated red light fractions. For any given red light fraction around the optimum (30 % to 90 % red light), attributing the remaining illumination intensity to blue light instead of green light leads to higher expected optical densities. Under these conditions, static excitation of PSI by blue light photons could be counteracted by red light, primarily causing excitation of PSII through the allophycocyanin core of the phycobilisomes at a wavelength of 660 nm [13,60]. Green light, on the other hand, is not optimally utilized by any of the major light-harvesting pigments, chlorophyll *a*, allophycocyanin, or phycocyanin in *Synechocystis sp.* [7]. Nonetheless, if the red light fraction is minimized, green light leads to better growth performance than blue light. For 100 % green light, the model predicts a mean optical density of 6.53, whereas the predicted mean optical density lies at 5.18 for 100 % blue light. These observations are in agreement with previous studies of monochromatically illuminated cultures of *Synechocystis* 6803 [7,40].

The contour plots for the respective models for the endpoint squalene concentration and the cellular squalene load are depicted in Fig. 3. Here, UV-A light was included as a factor in the model because the supplementation of UV-A light had a significant effect on the observed squalene concentration. Fig. 3 shows the respective model prediction for cultivations with 1 $\mu mol_{Photons}\ m^{-2}\ s^{-1}$ UV-A light (A and C) and without UV-A supplementation (B and D). The overall model fit for the response of the endpoint squalene concentration depicted in Fig. 3A and B resulted in an R^2 of 0.82 and a *p*-value of < 0.001, while the model for the cellular squalene load shown in Fig. 3C and D had an R^2 of 0.78 and a *p*-value of 0.002. The highest mean endpoint squalene concentration of approximately 48.2 $mg\ L^{-1}$ (95 % CI [34.8, 61.6] $mg\ L^{-1}$) was predicted for a mixture of approximately 63 % red, 0 % green, and 37 % blue light irradiation if the culture is simultaneously supplemented with UV-A light. This approximately coincides with the optimal mixture of light colors that was predicted for the endpoint optical density. If no UV-A light is supplied, the predicted squalene concentration is greatly reduced, as shown in Fig. 3B. The local optimum in this case lies at a predicted value of 40.6 $mg\ L^{-1}$ (95 % CI [27.1, 54.1] $mg\ L^{-1}$). Interestingly, compared to the condition with UV-A supplementation, the optimum lies at an increased blue light fraction of approximately 56 % and a reduced red light fraction of approximately 44 %. This trend is explained by the dependence of the cellular squalene load on light color (Fig. 3C and D). If no UV-A light is supplied to the culture, the squalene load decreases with increasing red light fraction, while the relative amount of blue or green light is predicted to have little effect. Thus, the optimum shown in Fig. 3B lies at the intersection of optimizing squalene load and biomass concentration. Contrastingly, supplementing only a low amount of UV-A irradiation appears to stimulate the synthesis of squalene in the region of elevated red light fractions (Fig. 3C). This leads to the common optimum for both optical density and squalene concentration under UV-A supplementation. It should be noted that the limitations of the experimental design do not allow us to fully separate a wavelength-dependent effect of the UV-A supplementation from the simultaneous increase in total photon input (40 $\mu mol_{Photons}\ m^{-2}\ s^{-1}$ vs. 41 $\mu mol_{Photons}\ m^{-2}\ s^{-1}$). However, it is unlikely that the observed elevated squalene concentration under UV-A supplementation is a result purely of the additional energy input, since UV-A radiation was shown to generally decrease photosynthetic efficiency in *Synechocystis* 6803 and does not account for the photosynthetically active radiation [61,62]. The highest experimentally observed squalene concentration was at 47.35 $mg\ L^{-1}$ for a factor setting of 70 % red and 30 % blue light irradiation with added UV-A light. This single observation and the near predicted mean of the optimum exceed

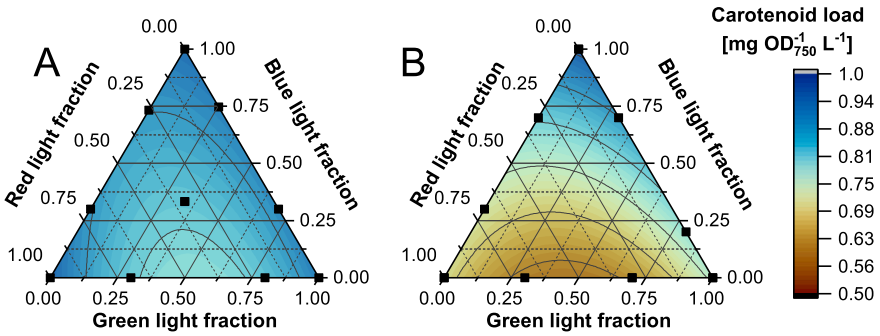

Fig. 4. Contour plots of model predictions for the cellular carotenoid load of cultivations with different wavelength compositions. In total, the photosynthetically active illumination intensity sums up to 40 $\mu mol_{Photons}\ m^{-2}\ s^{-1}$ for all conditions. A: UV-A light (365 nm) was supplied to the culture at an illumination intensity of 1 $\mu mol_{Photons}\ m^{-2}\ s^{-1}$; B: No UV-A light supplementation. A varying amount of red (660 nm), blue (451 nm), or green (528 nm) light was provided to the culture. The model was fit based on Eq. (4). A summary of the model parameters is given in the supplementary material, Table S6. The studentized residuals are plotted in the supplementary material, Figure S6D. Overall, 23 data points were used that were randomly distributed into 3 separate experimental blocks. Settings of the performed experiments are indicated by black squares in the plot.

the previously reported concentration of 13 $mg\ L^{-1}$ [35] by more than threefold.

Cellular chlorophyll *a* and carotenoid loads are important variables for squalene synthesis in cyanobacteria. Since these pigments are at least partially derived from the MEP pathway, their cellular loads, together with the production of squalene, are indicative of the pathway's activity. Moreover, due to the common precursors of the phytol tail of chlorophyll *a*, carotenoids, and squalene, it is important to assess competition for carbon between these products under different conditions [30,33]. Cellular chlorophyll *a* and carotenoid loads are further indicative of a photooxidative stress response and thus display the vitality of the cells [63,64]. Hence, we also determined the concentrations of carotenoids and chlorophyll *a* for all performed cultivations. The cellular chlorophyll *a* load was not significantly influenced by the ratios of red, blue, and green light or the supplementation of UV-A light. We registered a chlorophyll *a* load of $3.06 \pm 0.44\ mg\ OD_{750}^{-1}\ L^{-1}$ at the endpoint across all 23 tested conditions. For the cellular carotenoid load, on the other hand, we could fit a model based on Eq. (4) with an R^2 of 0.81 and a *p*-value of < 0.0001. The corresponding contour plot is shown in Fig. 4. If no UV-A irradiation is supplied to the culture (Fig. 4B), we observed an increase in the cellular carotenoid load with an increase in the fraction of blue light. The carotenoid load was minimized for conditions without blue light and medium amounts of red and green light if no UV-A light was supplied. Elevating the red light fraction compared to the green light fraction under low blue light and no UV-A supplementation led to an increase in the cellular carotenoid load. This effect differs for the response of the cellular squalene load and manifests in lowered squalene-to-carotenoid ratios under predominant red light conditions. For UV-A-treated cultures, the region where the carotenoid load was minimized is similar to the region for conditions without UV-A supplementation (Fig. 4A). However, the minimum value of approximately $0.80\ mg\ OD_{750}^{-1}\ L^{-1}$, expected under UV-A supplementation, is only realized for high blue and low red light fractions if no UV-A light is supplied. It should be noted that the full data set models (supplementary material, Figure S4C and S5A) suggest a lowered squalene and carotenoid load for high blue light fractions under UV-A supplementation. Thus, it cannot be excluded that UV-A supplementation has a detrimental effect at elevated blue light levels.

Overall, the presented results are in accordance with earlier reports that carotenoid synthesis is promoted by low-dosage UV-A irradiation in cyanobacteria [58,59] and further suggest that blue light similarly increases the synthesis of carotenoids in *Synechocystis Δshc sqs* +3MEP. Together with the results for squalene concentration (Fig. 3), we can further infer that the synthesis of carotenoids and squalene show a similar response pattern in the tested design space, especially regarding the effects of UV-A supplementation and elevated blue light fractions. In contrast, high red light fractions with no UV-A supplementation appear to inhibit squalene synthesis in relation to carotenoids, leading to a lower squalene-to-carotenoid ratio. Overall, irradiation with blue light or supplementation with UV-A light could potentially be exploited to increase the production of both squalene and carotenoids with *Synechocystis sp.*, but favoring squalene over carotenoid production appears to be not possible under the tested cultivation conditions.

3.3. Optimizing the illumination intensity profile and endpoint incident illumination intensity for growth and squalene production

Besides the effect of different mixtures of monochromatic light, we were interested in the effect of maximum illumination intensity and illumination intensity profiles. Thus, the effect of incrementally increasing the illumination intensity of a white light LED to different maximum illumination intensities was investigated. The illumination intensity was increased either at a rate below (photo-limited) or above (photo-saturated) the potential growth rate of the organism. The limiting rate of increase was previously determined from the continuously recorded oxygen transfer rate during growth of *Synechocystis Δshc sqs* +3MEP (Figure S7). Additionally, we tested both the induced and uninduced state of product synthesis to assess differences in sensitivity to higher illumination intensities. The induced state refers to cultures treated with 5 mM L-rhamnose, inducing the expression of three MEP pathway genes and the gene encoding the squalene synthase in the production strain. In total, we performed 48 parallel cultivations over the course of approximately 7 d in a μRAMOS system equipped with an LED module [47].

The difference between a photo-limited or photo-saturated increase in illumination intensity on growth, product synthesis, and cellular pigment loads was mostly non-significant in the induced state of the strain. However, the models for the endpoint carotenoid and chlorophyll *a* load had a weakly significant active interaction effect between the maximum illumination intensity and the slope of the illumination intensity increase at p-values < 0.05. Given the negative parameter estimate in both models, a higher cellular pigment load is expected when illumination intensity increases slowly, particularly at high maximum illumination intensities. For the model graphs depicted in Fig. 5, we thus fixed the level for the slope of illumination intensity increase at the center point level ($4\ \mu mol_{Photons}\ m^{-2}\ s^{-1}\ h^{-1}$) for all graphs. Fig. 5A compares the endpoint optical density for different tested maximum illumination intensities and different states of induction. The endpoint optical density increases between the lower and center point settings for both induction states and moderately decreases between the center point and the higher maximum illumination intensity settings. While the predicted maximum optical density is slightly higher for the

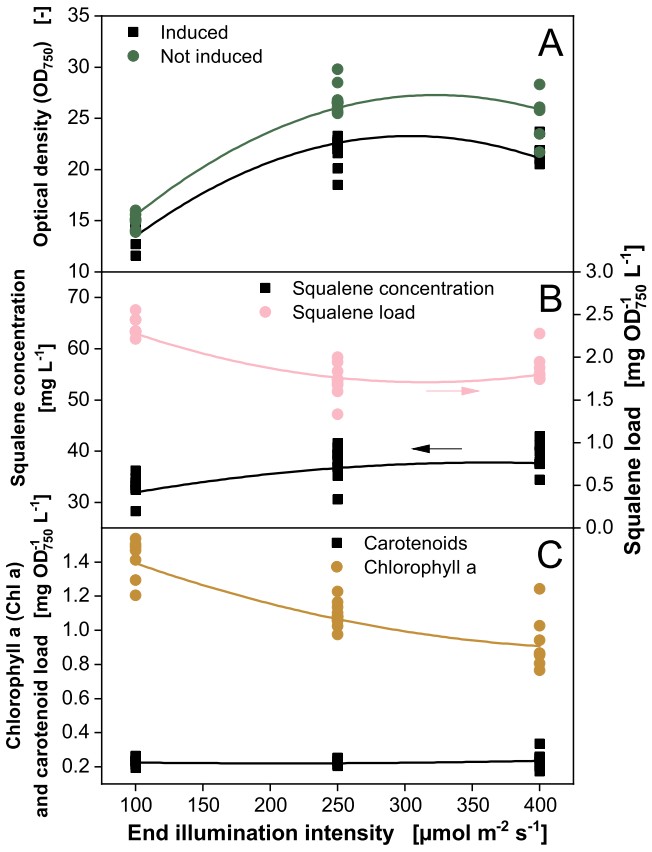

Fig. 5. Observed data and model fit for cultivations under different maximum illumination intensities and induction states. A: Comparison of the endpoint optical density for cultures that were either induced or not induced with 5 mM L-rhamnose; B: Cellular squalene load and endpoint squalene concentration as a function of maximum illumination intensity; C: Cellular chlorophyll *a* and carotenoid load of cells grown under varying maximum illumination intensity. The squalene concentration was determined by the HPLC method described in Section 2.6. Each response was fit individually to the model given in Eq. (5). Summaries of the model parameters are given in the supplementary material, Table S8-S12. The level of the illumination intensity increase was fixed at the center point level (4 $\mu mol_{Photons}\ m^{-2}\ s^{-1}\ h^{-1}$) for all models.

uninduced state at a value of 27.27 compared to the value of 23.27, the location of the optimum is nearly identical for both states. This indicates comparable sensitivity to the tested maximum illumination intensity between both states. The overall lower optical density could be attributed to higher levels of carbon flux being partitioned to synthesize squalene in the induced condition. However, we did not measure intracellular carbon fluxes to test this hypothesis.

Fig. 5B displays how the endpoint squalene concentration and cellular squalene load change with respect to different maximum illumination intensities. The model for the squalene concentration resulted in an R^2 of 0.91, while the model for the squalene load exhibited an R^2 of 0.94. Generally, the trend of endpoint squalene concentration follows the trend that was recorded for the endpoint optical density, though the increase in squalene concentration is less pronounced than that of the endpoint optical density. This results in an increased predicted squalene load of 2.28 $mg\ OD_{750}^{-1}\ L^{-1}$ at lower maximum illumination intensities. Despite the increase in squalene load for lower maximum illumination intensities, the maximum squalene concentration is expected to be reached near illumination intensities that result in maximal biomass concentration.

It should be noted that the maximum predicted squalene load is lower than the value of $3.85 \pm 0.75\ mg\ OD_{750}^{-1}\ L^{-1}$ that was recorded for the cultivation under white light in shake flasks (Fig. 1). However, this cultivation was conducted with a considerably lower constant illumination intensity of 30 $\mu mol_{Photons}\ m^{-2}\ s^{-1}$ in a different cultivation set-up. Though the trend shown in Fig. 5B might also hold for lower illumination intensities, the sizable difference in the CO_2 in-gas concentrations between shake flask- and microtiter plate-scale (1.5 % vs. 5 %) and differences in light distribution in both cultivation set-ups render a direct comparison of response values infeasible. While we do not expect a CO_2 transfer limitation for both cultivation set-ups, a different CO_2 equilibrium concentration in the medium and differences in light distribution are expected to affect the photosynthetic activity at a given incident illumination intensity differently between both systems [65].

The trends for the chlorophyll *a* and carotenoid load with respect to the applied maximum illumination intensity are displayed in Fig. 5C. The underlying models had an R^2 of 0.75 and 0.66, respectively. The chlorophyll *a* load was observed to decrease with increasing maximum illumination intensity. Contrastingly, the carotenoid load did not significantly change with increasing maximum illumination intensity. One possible explanation for the observed constant carotenoid load in the design space could be that the cells are not significantly stressed by the applied light, though a physiological stress response cannot be fully excluded based on the presented results [66]. The effect of chlorophyll *a* load decreasing concurrently with increasing illumination intensity had previously been shown for other species of cyanobacteria [67,68]. Therefore, regarding the factor of endpoint illumination intensity under white light, the cellular squalene load appears to be correlated more with elevated chlorophyll *a* synthesis than the elevated carotenoid levels that were observed when applying higher blue light fractions or supplementing the culture with low-dosage UV-A light.

Overall, for white light illumination in batch production, setting the illumination intensity to achieve optimal biomass concentrations appears to be the most effective strategy to maximize squalene concentration. Nonetheless, supplementing the illumination of the culture with UV-A light showed promising results at the lower illumination intensities that were necessarily applied in the shake flask experiments. Since a direct comparison between shake flask and microtiter plate results is not possible due to scale and potential CO_2 concentration effects, yet general trends concerning the light intensity are expected to hold between systems, an investigation of the effect of UV-A supplementation or elevated blue light fractions at higher incident illumination intensities might yield positive results in future studies.

4. Conclusion

The results of this work underline the importance of optimizing and controlling the spectral composition of the incident illumination in cyanobacterial cultures. We found that mixtures of wavelengths from distant spectral regions perform more optimally than monochromatic light sources for the genetically engineered strain *Synechocystis Δshc sqs* +3MEP, regarding both biomass and squalene synthesis. While elevated red light fractions led to an increased biomass concentration, the addition of more blue light improved cellular squalene loads. The potentially antagonistic nature of the effect of blue and red light poses a great possibility for process optimization by improving resource allocation between biomass and product synthesis during cultivation. Additionally, low-dosage UV-A supplementation stimulated terpenoid synthesis in the form of carotenoids and squalene under elevated red light fractions without compromising biomass growth. Thereby, UV-A light supplementation alleviates the necessity for balancing biomass and squalene production occurring during irradiation with only photosynthetically active photons. Here, future research could take a deeper look at how increasing dosage or different types of UV irradiation affect the optimal setting for squalene synthesis. Higher white light intensities led to a decrease in squalene load. However, the coinciding increase in biomass concentration resulted in the optimal squalene concentration

corresponding to the same maximum illumination intensity as the optimal biomass concentration. Hence, while optimizing the illumination intensity is still necessary, it appears to yield less significance for the control of squalene production than the spectral composition of the applied light source.

The transition from laboratory-scale screening to industrial-scale squalene production with cyanobacteria requires addressing several critical challenges related to the durability and sustainability of photosynthetic processes. The primary challenge lies in controlling illumination conditions at scale. In large-scale outdoor photosynthetic production, maintaining optimal spectral composition and light intensity would require either supplementation with LEDs or installation of optical filters to compensate for natural sunlight fluctuations. Conversely, indoor cultivation with fully controlled artificial lighting incurs substantial operational costs. The viability of the proposed light-regime approach thus hinges on whether the documented productivity gains justify these adaptations relative to uncontrolled outdoor cultivation. In the context of light optimization, it will be essential to assess biological and technical limitations for sustained long-term productivity under the proposed and derived cultivation conditions. While oxidative degradation of squalene during extended cultivation under high-photon-energy light regimes could potentially be managed through *in situ* product removal or microoxic operation, genetic stability of the production strain, including optimized genetic engineering strategies designed for industrial large-scale processes and approaches targeting growth-coupled production, represents an additional consideration requiring dedicated experimental validation. While these questions fall beyond the scope of the present proof-of-concept study, they are essential for evaluating the industrial feasibility of photoautotrophic terpenoid production.

CRediT authorship contribution statement

Leon Poduschnick: Writing – original draft, Visualization, Methodology, Investigation, Formal analysis, Conceptualization. **David Mihaescu:** Investigation. **Andreas Nakielski:** Methodology. **Dennis Dienst:** Writing – review & editing. **Ann-Katrin Beuel:** Resources, Methodology, Funding acquisition. **Leonie Voß:** Resources, Methodology. **Ilka Maria Axmann:** Writing – review & editing, Supervision, Project administration, Funding acquisition, Conceptualization. **Jørgen Barsett Magnus:** Writing – review & editing, Supervision, Resources, Project administration.

Funding

Open Access funding was enabled and organized by Projekt DEAL. The scientific activities of the Bioeconomy Science Center were financially supported by the Ministry of Culture and Science within the framework of the NRW Strategieprojekt BioSC (No. 005-2012-0107) in the SEED FUND 3.0 project LEDCyans. Funded by the Deutsche Forschungsgemeinschaft (DFG, German Research Foundation) – SFB1535 - Project ID 458090666.

Declaration of competing interest

The authors declare that they have no known competing financial interests or personal relationships that could have appeared to influence the work reported in this paper.

Acknowledgments

The authors would like to thank the Fraunhofer Institute for Molecular Biology and Applied Ecology (IME) for providing a prototype of the LEDitSHAKE module (European Patent EP3787784B1) to the Chair of Biochemical Engineering for the duration of the research project. Parts of the graphical abstract were created in BioRender. Magnus, J. (2026) https://BioRender.com/fmhz1vf, https://BioRender.com/859nppw,

Appendix A. Supplementary data

Supplementary material related to this article can be found online at https://doi.org/10.1016/j.algal.2026.104999.

Data availability

Data will be made available on request.

References

[1] Q. Huang, F. Jiang, L. Wang, C. Yang, Design of photobioreactors for mass cultivation of photosynthetic organisms, Engineering 3 (3) (2017) 318–329, http://dx.doi.org/10.1016/J.ENG.2017.03.020.
[2] C.W. Kim, M.-G. Sung, K. Nam, M. Moon, J.-H. Kwon, J.-W. Yang, Effect of monochromatic illumination on lipid accumulation of nannochloropsis gaditana under continuous cultivation, Bioresour. Technol. 159 (2014) 30–35, http://dx.doi.org/10.1016/j.biortech.2014.02.024.
[3] W. Blanken, M. Cuaresma, R.H. Wijffels, M. Janssen, Cultivation of microalgae on artificial light comes at a cost, Algal Res. 2 (4) (2013) 333–340, http://dx.doi.org/10.1016/j.algal.2013.09.004.
[4] M.D. Ooms, P.J. Graham, B. Nguyen, E.H. Sargent, D. Sinton, Light dilution via wavelength management for efficient high-density photobioreactors, Biotechnol. Bioeng. 114 (6) (2017) 1160–1169, http://dx.doi.org/10.1002/bit.26261.
[5] B.L. Montgomery, Seeing new light: recent insights into the occurrence and regulation of chromatic acclimation in cyanobacteria, Curr. Opin. Plant Biol. 37 (2017) 18–23, http://dx.doi.org/10.1016/j.pbi.2017.03.009.
[6] L.B. Wiltbank, D.M. Kehoe, Diverse light responses of cyanobacteria mediated by phytochrome superfamily photoreceptors, Nat. Rev. Microbiol. 17 (1) (2019) 37–50, http://dx.doi.org/10.1038/s41579-018-0110-4.
[7] T. Zavřel, A. Segečová, L. Kovács, M. Lukeš, Z. Novák, A.-C. Pohland, M. Szabó, B. Somogyi, O. Prášil, J. Červený, G. Bernát, A comprehensive study of light quality acclimation in Synechocystis Sp. PCC 6803, Plant Cell Physiol. 65 (8) (2024) 1285–1297, http://dx.doi.org/10.1093/pcp/pcae062.
[8] M. Kubushiro, T. Otsu, N. Misawa, M. Hamada, T. Eki, S. Kawai, Y. Hirose, Partial photoswitching of rod-shaped phycobilisome production in the cyanobacterium Synechocystis sp. PCC 6803, Plant Cell Physiol. 66 (9) (2025) 1274–1283, http://dx.doi.org/10.1093/pcp/pcaf064.
[9] Y. Hirose, T. Shimada, R. Narikawa, M. Katayama, M. Ikeuchi, Cyanobacteriochrome CcaS is the green light receptor that induces the expression of phycobilisome linker protein, Proc. Natl. Acad. Sci. USA 105 (28) (2008) 9528–9533, http://dx.doi.org/10.1073/pnas.0801826105.
[10] R.M.W. Chau, D. Bhaya, K.C. Huang, Emergent phototactic responses of cyanobacteria under complex light regimes, MBio 8 (2) (2017) http://dx.doi.org/10.1128/mbio.02330-16.
[11] Y. Sugimoto, H. Nakamura, S. Ren, K. Hori, S. Masuda, Genetics of the blue light-dependent signal cascade that controls phototaxis in the cyanobacterium Synechocystis sp. PCC6803, Plant Cell Physiol. 58 (3) (2017) 458–465, http://dx.doi.org/10.1093/pcp/pcw218.
[12] T. Zavřel, P. Očenášová, J. Červený, Phenotypic characterization of Synechocystis sp. PCC 6803 substrains reveals differences in sensitivity to abiotic stress, PLoS One 12 (12) (2017) e0189130, http://dx.doi.org/10.1371/journal.pone.0189130.
[13] V.M. Luimstra, J.M. Schuurmans, A.M. Verschoor, K.J. Hellingwerf, J. Huisman, H.C.P. Matthijs, Blue light reduces photosynthetic efficiency of cyanobacteria through an imbalance between photosystems I and II, Photosynth. Res. 138 (2) (2018) 177–189, http://dx.doi.org/10.1007/s11120-018-0561-5.
[14] C.-Y. Wang, C.-C. Fu, Y.-C. Liu, Effects of using light-emitting diodes on the cultivation of Spirulina platensis, Biochem. Eng. J. 37 (1) (2007) 21–25, http://dx.doi.org/10.1016/j.bej.2007.03.004.
[15] V.M. Luimstra, J.M. Schuurmans, K.J. Hellingwerf, H.C.P. Matthijs, J. Huisman, Blue light induces major changes in the gene expression profile of the cyanobacterium Synechocystis sp. PCC 6803, Physiol. Plant. 170 (1) (2020) 10–26, http://dx.doi.org/10.1111/ppl.13086.
[16] A. Cordara, A. Re, C. Pagliano, P. van Alphen, R. Pirone, G. Saracco, F. Branco Dos Santos, K. Hellingwerf, N. Vasile, Analysis of the light intensity dependence of the growth of Synechocystis and of the light distribution in a photobioreactor energized by 635 nm light, PeerJ 6 (2018) e5256, http://dx.doi.org/10.7717/peerj.5256.
[17] C. Posten, S. Feng Chen, Microalgae Biotechnology, vol. 153, Springer International Publishing, Cham, 2016, http://dx.doi.org/10.1007/978-3-319-23808-1.
[18] P. Benner, L. Meier, A. Pfeffer, K. Krüger, J.E. Oropeza Vargas, D. Weuster-Botz, Lab-scale photobioreactor systems: principles, applications, and scalability, Bioprocess Biosyst. Eng. 45 (5) (2022) 791–813, http://dx.doi.org/10.1007/s00449-022-02711-1.
[19] H. Morschett, V. Loomba, G. Huber, W. Wiechert, E. von Lieres, M. Oldiges, Laboratory-scale photobiotechnology-current trends and future perspectives, FEMS Microbiol. Lett. 365 (1) (2018) http://dx.doi.org/10.1093/femsle/fnx238.

[20] T.J. Johnson, S. Katuwal, G.A. Anderson, L. Gu, R. Zhou, W.R. Gibbons, Photobioreactor cultivation strategies for microalgae and cyanobacteria, Biotechnol. Prog. 34 (4) (2018) 811–827, http://dx.doi.org/10.1002/btpr.2628.
[21] F. Pagels, J. Bonomi-Barufi, J. Vega, R. Abdala-Díaz, V. Vasconcelos, A.C. Guedes, F.L. Figueroa, Light quality triggers biochemical modulation of cyanobium sp.—photobiology as tool for biotechnological optimization, J. Appl. Phycol. 32 (5) (2020) 2851–2861, http://dx.doi.org/10.1007/s10811-020-02179-0.
[22] W. Chen, S. Xu, S. Zou, Z. Liu, Y. Liu, H. Xu, J. Wang, J. Ma, R. Chen, Z. Zuo, Carbohydrate and lipid yield in microcystis aeruginosa for biofuel production under different light qualities, Biotechnol. Biofuels Bioprod. 18 (1) (2025) 36, http://dx.doi.org/10.1186/s13068-025-02615-8.
[23] E.A. Suyono, Aminin, L. Pradani, U. Mu'avatun, R.N. Habiba, Ramdaniyah, E.F. Rohma, Combination of blue, red, white, and ultraviolet lights for increasing carotenoids and biomass of microalga haematococcus pluvialis, Procedia Environ. Sci. 28 (2015) 399–405, http://dx.doi.org/10.1016/j.proenv.2015.07.049.
[24] M. Zeeshan, S.M. Prasad, Differential response of growth, photosynthesis, antioxidant enzymes and lipid peroxidation to UV-B radiation in three cyanobacteria, S. Afr. J. Bot. 75 (3) (2009) 466–474, http://dx.doi.org/10.1016/j.sajb.2009.03.003.
[25] M. Kokabi, M. Yousefzadi, M. Soltani, M. Arman, Effects of different UV radiation on photoprotective pigments and antioxidant activity of the hot–spring cyanobacterium Leptolyngbya cf. fragilis, Phycol. Res. 67 (3) (2019) 215–220, http://dx.doi.org/10.1111/pre.12374.
[26] J. Assunção, F. Pagels, T. Tavares, F.X. Malcata, A.C. Guedes, Light modulation for bioactive pigment production in Synechocystis salina, Bioeng. (Basel, Switzerland) 9 (7) (2022) http://dx.doi.org/10.3390/bioengineering9070331.
[27] T. Izuhara, I. Kaihatsu, H. Jimbo, S. Takaichi, Y. Nishiyama, Elevated levels of specific carotenoids during acclimation to strong light protect the repair of photosystem II in Synechocystis sp. PCC 6803, Front. Plant Sci. 11 (2020) 1030, http://dx.doi.org/10.3389/fpls.2020.01030.
[28] S. Steiger, L. Schäfer, G. Sandmann, High-light-dependent upregulation of carotenoids and their antioxidative properties in the cyanobacterium Synechocystis PCC 6803, J. Photochem. Photobiol. B 52 (1–3) (1999) 14–18, http://dx.doi.org/10.1016/S1011-1344(99)00094-9.
[29] C.C.C.R. de Carvalho, M.M.R. Da Fonseca, Biotransformation of terpenes, Biotech. Adv. 24 (2) (2006) 134–142, http://dx.doi.org/10.1016/j.biotechadv.2005.08.004.
[30] A. Banerjee, T.D. Sharkey, Methylerythritol 4-phosphate (MEP) pathway metabolic regulation, Nat. Prod. Rep. 31 (8) (2014) 1043–1055, http://dx.doi.org/10.1039/C3NP70124G.
[31] O. Klaus, F. Hilgers, A. Nakielski, D. Hasenklever, K.-E. Jaeger, I.M. Axmann, T. Drepper, Engineering phototrophic bacteria for the production of terpenoids, Curr. Opin. Biotechnol. 77 (2022) 102764, http://dx.doi.org/10.1016/j.copbio.2022.102764.
[32] N. Gohil, G. Bhattacharjee, K. Khambhati, D. Braddick, V. Singh, Engineering strategies in microorganisms for the enhanced production of squalene: Advances, challenges and opportunities, Front. Bioeng. Biotechnol. 7 (2019) 50, http://dx.doi.org/10.3389/fbioe.2019.00050.
[33] B. Pattanaik, P. Lindberg, Terpenoids and their biosynthesis in cyanobacteria, Life (Basel, Switzerland) 5 (1) (2015) 269–293, http://dx.doi.org/10.3390/life5010269.
[34] P.-C. Lin, F. Zhang, H.B. Pakrasi, Enhanced limonene production in a fast-growing cyanobacterium through combinatorial metabolic engineering, Metab. Eng. Commun. 12 (2021) e00164, http://dx.doi.org/10.1016/j.mec.2021.e00164.
[35] A.T. Germann, A. Nakielski, M. Dietsch, T. Petzel, D. Moser, A systematic overexpression approach reveals native targets to increase squalene production in Synechocystis, Front. Plant Sci. Volume 14 (2023).
[36] S.Y. Choi, J.-Y. Wang, H.S. Kwak, S.-M. Lee, Y. Um, Y. Kim, S.J. Sim, J.-I. Choi, H.M. Woo, Improvement of squalene production from CO2 in synechococcus elongatus PCC 7942 by metabolic engineering and scalable production in a photobioreactor, ACS Synth. Biol. 6 (7) (2017) 1289–1295, http://dx.doi.org/10.1021/acssynbio.7b00083.
[37] S.Y. Choi, S.J. Sim, S.C. Ko, J. Son, J.S. Lee, H.J. Lee, W.S. Chang, H.M. Woo, Scalable cultivation of engineered cyanobacteria for squalene production from industrial flue gas in a closed photobioreactor, J. Agricult. Food Chem. 68 (37) (2020) 10050–10055, http://dx.doi.org/10.1021/acs.jafc.0c03133.
[38] E. Englund, B. Pattanaik, S.J.K. Ubhayasekera, K. Stensjö, J. Bergquist, P. Lindberg, Production of squalene in Synechocystis sp. PCC 6803, PLoS One 9 (3) (2014) e90270, http://dx.doi.org/10.1371/journal.pone.0090270.
[39] M. Dietsch, A. Behle, P. Westhoff, I.M. Axmann, Metabolic engineering of Synechocystis sp. PCC 6803 for the photoproduction of the sesquiterpene valencene, Metab. Eng. Commun. 13 (2021) e00178, http://dx.doi.org/10.1016/j.mec.2021.e00178.
[40] J.S. Rodrigues, L. Kovács, M. Lukeš, R. Höper, R. Steuer, J. Červený, P. Lindberg, T. Zavřel, Characterizing isoprene production in cyanobacteria - Insights into the effects of light, temperature, and isoprene on Synechocystis sp. PCC 6803, Bioresour. Technol. 380 (2023) 129068, http://dx.doi.org/10.1016/j.biortech.2023.129068.
[41] J.S. Rodrigues, P. Lindberg, Metabolic engineering of Synechocystis sp. PCC 6803 for improved bisabolene production, Metab. Eng. Commun. 12 (2021) e00159, http://dx.doi.org/10.1016/j.mec.2020.e00159.
[42] K.N. Janssen, P. Bolay, A. Tüllinghoff, J. Toepel, D. Spindler, B. Bühler, P. Lindberg, Engineering cyanobacteria for high-yield photosynthetic isoprene production with long-term phenotypic stability, Plant Biotech. J. 24 (3) (2026) 1014–1030, http://dx.doi.org/10.1111/pbi.70395.
[43] L. Lippi, L. Bähr, A. Wüstenberg, A. Wilde, R. Steuer, Exploring the potential of high-density cultivation of cyanobacteria for the production of cyanophycin, Algal Res. 31 (2018) 363–366, http://dx.doi.org/10.1016/j.algal.2018.02.028.
[44] A.-K. Beuel, N. Jablonka, J. Heesel, K. Severin, H. Spiegel, S. Rasche, LEDit-SHAKE: a lighting system to optimize the secondary metabolite content of plant cell suspension cultures, Sci. Rep. 11 (1) (2021) 23353, http://dx.doi.org/10.1038/s41598-021-02762-6.
[45] A.-K. Beuel, LEDitGROW - Beleuchtungssysteme zur Optimierung von Pflanzenzellkulturen für die Sekundärmetabolit-Produktion (Dissertation), Lehrstuhl für Molekulare Biotechnologie; Fachgruppe Biologie, RWTH Aachen University, Aachen, 2022, http://dx.doi.org/10.18154/RWTH-2022-09555.
[46] D. Flitsch, S. Krabbe, T. Ladner, M. Beckers, J. Schilling, S. Mahr, U. Conrath, W.K. Schomburg, J. Büchs, Respiration activity monitoring system for any individual well of a 48-well microtiter plate, J. Biol. Eng. 10 (2016) 14, http://dx.doi.org/10.1186/s13036-016-0034-3.
[47] J. Loogen, A. Müller, A. Balzer, S. Weber, K. Schmitz, R. Krug, U. Schaffrath, J. Pietruszk, U. Conrath, J. Büchs, An illuminated respiratory activity monitoring system identifies priming-active compounds in plant seedlings, BMC Plant Biol. 21 (1) (2021) 324, http://dx.doi.org/10.1186/s12870-021-03100-8.
[48] R.J. Ritchie, Consistent sets of spectrophotometric chlorophyll equations for acetone, methanol and ethanol solvents, Photosynth. Res. 89 (1) (2006) 27–41, http://dx.doi.org/10.1007/s11120-006-9065-9.
[49] A.R. Wellburn, The spectral determination of chlorophylls a and b, as well as total carotenoids, using various solvents with spectrophotometers of different resolution, J. Plant Physiol. 144 (3) (1994) 307–313, http://dx.doi.org/10.1016/S0176-1617(11)81192-2.
[50] H. Matsuura, M.M. Watanabe, K. Kaya, Squalene quantification using octadecylbenzene as the internal standard, Procedia Environ. Sci. 15 (2012) 43–46, http://dx.doi.org/10.1016/j.proenv.2012.05.008.
[51] D.C. Montgomery, Design and Analysis of Experiments, ninth ed., Wiley, Hoboken, NJ, 2017.
[52] L. Brown, A.N. Donev, A.C. Bissett, General blending models for data from mixture experiments, Technometrics 57 (4) (2015) 449–456, http://dx.doi.org/10.1080/00401706.2014.947003.
[53] S. Kowalski, J.A. Cornell, G. Geoffrey Vining, A new model and class of designs for mixture experiments with process variables, Comm. Statist. Theory Methods 29 (9–10) (2000) 2255–2280, http://dx.doi.org/10.1080/03610920008832606.
[54] T. Anderlei, J. Büchs, Device for sterile online measurement of the oxygen transfer rate in shaking flasks, Biochem. Eng. J. 7 (2) (2001) 157–162, http://dx.doi.org/10.1016/S1369-703X(00)00116-9.
[55] A.K. Singh, M. Bhattacharyya-Pakrasi, T. Elvitigala, B. Ghosh, R. Aurora, H.B. Pakrasi, A systems-level analysis of the effects of light quality on the metabolism of a cyanobacterium, Plant Physiol. 151 (3) (2009) 1596–1608, http://dx.doi.org/10.1104/pp.109.144824.
[56] E. Bland, L.T. Angenent, Pigment-targeted light wavelength and intensity promotes efficient photoautotrophic growth of cyanobacteria, Bioresour. Technol. 216 (2016) 579–586, http://dx.doi.org/10.1016/j.biortech.2016.05.116.
[57] T. Pfennig, E. Kullmann, T. Zavřel, A. Nakielski, O. Ebenhöh, J. Červený, G. Bernát, A.B. Matuszyńska, Shedding light on blue-green photosynthesis: A wavelength-dependent mathematical model of photosynthesis in Synechocystis sp. PCC 6803, PLoS Comput. Biol. 20 (9) (2024) e1012445, http://dx.doi.org/10.1371/journal.pcbi.1012445.
[58] K. Gao, H. Yu, M.T. Brown, Solar PAR and UV radiation affects the physiology and morphology of the cyanobacterium Anabaena sp. PCC 7120, J. Photochem. Photobiol. B 89 (2–3) (2007) 117–124, http://dx.doi.org/10.1016/j.jphotobiol.2007.09.006.
[59] C.A. Llewellyn, R.L. Airs, G. Farnham, C. Greig, Synthesis, regulation and degradation of carotenoids under low level UV-b radiation in the filamentous cyanobacterium Chlorogloeopsis fritschii PCC 6912, Front. Microbiol. 11 (2020) 163, http://dx.doi.org/10.3389/fmicb.2020.00163.
[60] V.M. Luimstra, J.M. Schuurmans, C.F.M. de Carvalho, H.C.P. Matthijs, K.J. Hellingwerf, J. Huisman, Exploring the low photosynthetic efficiency of cyanobacteria in blue light using a mutant lacking phycobilisomes, Photosynth. Res. 141 (3) (2019) 291–301, http://dx.doi.org/10.1007/s11120-019-00630-z.
[61] S. Khanthasuwan, A. Incharoensakdi, S. Jantaro, Response of Synechocystis sp. PCC 6803 to UV radiations by alteration of polyamines associated with thylakoid membrane proteins, World J. Microbiol. Biotechnol. 35 (1) (2018) 8, http://dx.doi.org/10.1007/s11274-018-2580-y.
[62] P.R. Singh, A. Gupta, A.P. Singh, J. Jaiswal, R.P. Sinha, Effects of ultraviolet radiation on cellular functions of the cyanobacterium Synechocystis sp. PCC 6803 and its recovery under photosynthetically active radiation, J. Photochem. Photobiol. B. 252 (2024) 112866, http://dx.doi.org/10.1016/j.jphotobiol.2024.112866.
[63] Z. Mazur, I. Ślesak, Cyanobacteria under UV radiation: General insights into stress responses, Int. J. Mol. Sci. 26 (22) (2025) http://dx.doi.org/10.3390/ijms262210926.

[64] G. Cheloni, V.I. Slaveykova, Combined effects of trace metals and light on photosynthetic microorganisms in aquatic environment, Environments 5 (7) (2018) 81, http://dx.doi.org/10.3390/environments5070081.

[65] R.L. Burnap, M. Hagemann, A. Kaplan, Regulation of CO2 concentrating mechanism in cyanobacteria, Life (Basel, Switzerland) 5 (1) (2015) 348–371, http://dx.doi.org/10.3390/life5010348.

[66] M. Natesungnoen, V. Pongrakhananon, P. Lindblad, S. Jantaro, Overexpressing carotenoid biosynthetic genes in Synechocystis sp. PCC 6803 improved intracellular pigments and antioxidant activity, which can decrease the viability and proliferation of lung cancer cells in vitro, Int. J. Mol. Sci. 24 (11) (2023) http://dx.doi.org/10.3390/ijms24119370.

[67] N.U.F. Niangoran, D. Buso, G. Zissis, T. Prudhomme, Influence of light intensity and photoperiod on energy efficiency of biomass and pigment production of Spirulina (Arthrospira platensis), OCL 28 (2021) 37, http://dx.doi.org/10.1051/ocl/2021025.

[68] N. Soltani, R.A. Khavari-Nejad, M.T. Yazdi, S. Shokravi, E. Fernández-Valiente, Variation of nitrogenase activity, photosynthesis and pigmentation of the cyanobacterium fischerella ambigua strain FS18 under different irradiance and pH values, World J. Microbiol. Biotechnol. 22 (6) (2006) 571–576, http://dx.doi.org/10.1007/s11274-005-9073-5.